
# NAVAL POSTGRADUATE SCHOOL

**MONTEREY, CALIFORNIA**

# THESIS

**TERAHERTZ IMAGING VIA A MICROBOLOMETER CAMERA UNDER ILLUMINATION OF A QUANTUM CASCADE LASER**

by

Ioannis Nellas

December 2010

Thesis Co-Advisors

Gamani Karunasiri
Dragoslav Grbovic

**Approved for public release; distribution is unlimited**

THIS PAGE INTENTIONALLY LEFT BLANK

| REPORT DOCUMENTATION PAGE | | | Form Approved OMB No. 0704-0188 |
|---|---|---|---|
| Public reporting burden for this collection of information is estimated to average 1 hour per response, including the time for reviewing instruction, searching existing data sources, gathering and maintaining the data needed, and completing and reviewing the collection of information. Send comments regarding this burden estimate or any other aspect of this collection of information, including suggestions for reducing this burden, to Washington headquarters Services, Directorate for Information Operations and Reports, 1215 Jefferson Davis Highway, Suite 1204, Arlington, VA 22202-4302, and to the Office of Management and Budget, Paperwork Reduction Project (0704-0188) Washington DC 20503. | | | |
| **1. AGENCY USE ONLY** ***(Leave blank)*** | **2. REPORT DATE** December 2010 | **3. REPORT TYPE AND DATES COVERED** Master's Thesis | |
| **4. TITLE AND SUBTITLE** Terahertz Imaging Via a Microbolometer Camera Under the Illumination of a Quantum Cascade Laser | | **5. FUNDING NUMBERS** | |
| **6. AUTHOR(S)** Ioannis Nellas | | | |
| **7. PERFORMING ORGANIZATION NAME(S) AND ADDRESS(ES)** Naval Postgraduate School Monterey, CA 93943-5000 | | **8. PERFORMING ORGANIZATION REPORT NUMBER** | |
| **9. SPONSORING /MONITORING AGENCY NAME(S) AND ADDRESS(ES)** N/A | | **10. SPONSORING/MONITORING AGENCY REPORT NUMBER** | |
| **11. SUPPLEMENTARY NOTES** The views expressed in this thesis are those of the author and do not reflect the official policy or position of the Department of Defense or the U.S. Government. IRB Protocol number _____N/A_____. | | | |
| **12a. DISTRIBUTION / AVAILABILITY STATEMENT** Approved for public release; distribution is unlimited. | | **12b. DISTRIBUTION CODE** | |


**13. ABSTRACT (maximum 200 words)**

The terahertz (THz) region of the electromagnetic spectrum has not been fully utilized due to the lack of compact and efficient sources as well as detectors. This thesis aimed on characterizing a quantum cascade laser (QCL) beam and achieving high quality real-time THz imaging using a 160x120 pixel FLIR A20M microbolometer camera designed to operate in long wave infrared range. The FTIR spectroscopy of the QCL beam revealed that lasing could be achieved at 2.85 and 2.91 THz frequencies depending on the bias current. This behavior was analyzed using the longitudinal modes of the laser and found to correspond well with the experimental observations. Real-time imaging of concealed objects in transmission mode was accomplished using the silicon nitride-based microbolometer camera under illumination via the QCL with average power less than 1 mW. The larger extent of the object required the expansion of the narrow laser beam using a parabolic reflector and refocus on the camera using a second parabolic reflector. The standard Ge lens of the camera was replaced by a Tsurupica lens since the earlier lens was opaque to THz radiation. The real-time imaging can be extended to reflection mode as well as longer standoff distances using higher power THz lasers.


| **14. SUBJECT TERMS** QCL, Terahertz imaging, microbolometer, camera, Tsurupica lens, FLIR A20M, mode hopping, electrical tunability. | | | **15. NUMBER OF PAGES** 51 |
|---|---|---|---|
| | | | **16. PRICE CODE** |
| **17. SECURITY CLASSIFICATION OF REPORT** Unclassified | **18. SECURITY CLASSIFICATION OF THIS PAGE** Unclassified | **19. SECURITY CLASSIFICATION OF ABSTRACT** Unclassified | **20. LIMITATION OF ABSTRACT** UU |

NSN 7540-01-280-5500

Standard Form 298 (Rev. 2-89)
Prescribed by ANSI Std. 239-18

THIS PAGE INTENTIONALLY LEFT BLANK

**Approved for public release; distribution is unlimited**

# TERAHERTZ IMAGING VIA A MICROBOLOMETER CAMERA UNDER THE ILLUMINATION OF A QUANTUM CASCADE LASER

Ioannis Nellas
Lieutenant Junior Grade, Hellenic Navy
B.S., Hellenic Naval Academy, 2002

Submitted in partial fulfillment of the
requirements for the degree of

**MASTER OF SCIENCE IN APPLIED PHYSICS**

from the

**NAVAL POSTGRADUATE SCHOOL**
**December 2010**

Author: Ioannis Nellas

Approved by: Gamani Karunasiri
Thesis Advisor

Dragoslav Grbovic
Co-Advisor

Andres Larraza
Chairman, Department of Physics

THIS PAGE INTENTIONALLY LEFT BLANK

# ABSTRACT

The terahertz (THz) region of the electromagnetic spectrum has not been fully utilized due to the lack of compact and efficient sources as well as detectors. This thesis aimed on characterizing a quantum cascade laser (QCL) beam and achieving high quality real-time THz imaging using a 160x120 pixel FLIR A20M microbolometer camera designed to operate in long wave infrared range. The FTIR spectroscopy of the QCL beam revealed that lasing could be achieved at 2.85 and 2.91 THz frequencies depending on the bias current. This behavior was analyzed using the longitudinal modes of the laser and found to correspond well with the experimental observations. Real-time imaging of concealed objects in transmission mode was accomplished using the silicon nitride-based microbolometer camera under illumination via the QCL with average power less than 1 mW. The larger extent of the object required the expansion of the narrow laser beam using a parabolic reflector and refocus on the camera using a second parabolic reflector. The standard Ge lens of the camera was replaced by a Tsurupica lens since the earlier lens was opaque to THz radiation. The real-time imaging can be extended to reflection mode as well as longer standoff distances using higher power THz lasers.

THIS PAGE INTENTIONALLY LEFT BLANK

# TABLE OF CONTENTS

THIS PAGE INTENTIONALLY LEFT BLANK

# LIST OF FIGURES

THIS PAGE INTENTIONALLY LEFT BLANK

# LIST OF TABLES

THIS PAGE INTENTIONALLY LEFT BLANK

# LIST OF ACRONYMS AND ABBREVIATIONS

| | |
|---|---|
| AFOSR | Air Force Office of Scientific Research |
| FPA | Focal Plane Array |
| FTIR | Fourier Infrared Transform Spectroscopy |
| SRL | Sensor Research Laboratory |
| QCL | Quantum Cascade Laser |
| THz | Terahertz |
| TCR | Temperature Coefficient of Resistance |

THIS PAGE INTENTIONALLY LEFT BLANK

# ACKNOWLEDGMENTS

I would like to thank the Hellenic Navy for providing me the opportunity to study in the Physics Department of the Naval Postgraduate School. My studies here broadened my horizons, and the knowledge gained through the course of my studies in this institute will help me immensely in my future pursuits. Most importantly, I would like to express my deepest gratitude to my advisors, Dr. Karunasiri and Dr. Grbovic, for their tremendous support and understanding. In particular, Professor Karunasiri with his patience and insightful comments helped me get through this research journey and avoid reaching academic stalemates. This work is supported by AFOSR.

THIS PAGE INTENTIONALLY LEFT BLANK

# I. INTRODUCTION

Until recently, the terahertz (THz) sub-spectrum of the electromagnetic spectrum (see Figure 1) was not fully exploited or utilized, due to a lack of suitable sources and detectors. However, due to recent advances in the field, potential use of THz for imaging applications was demonstrated.

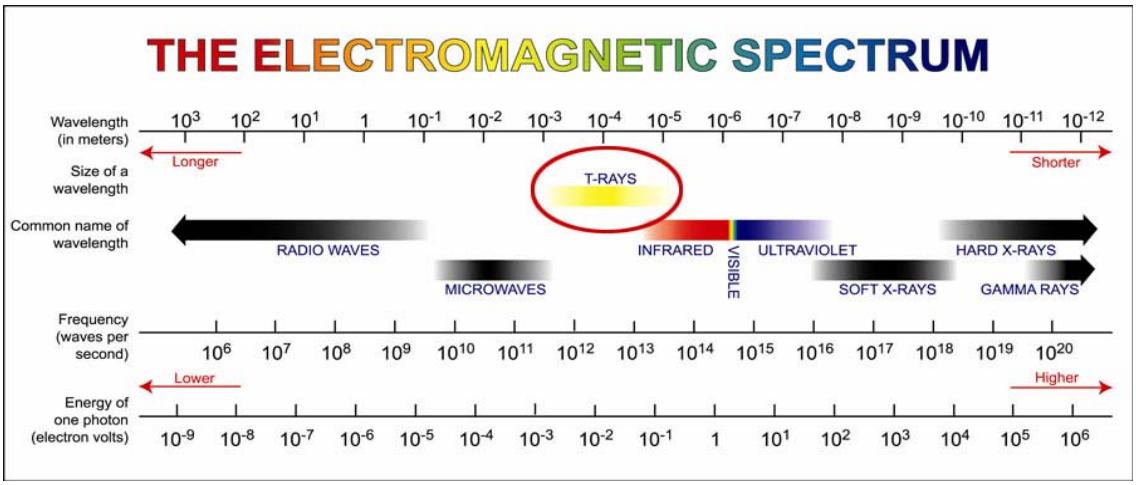


Figure 1. THz Radiation ("T-rays") with Respect to the Rest of the Electromagnetic Spectrum (From [1–2]).

These applications include detection of concealed objects and imaging of human tissue due to the special characteristics of this radiation. Specifically, the relatively long wavelength allows it to penetrate into the majority of nonmetallic materials and provides significant detection capability of metallic objects that are concealed in nonmetallic materials such as fabric, paper, and plastic (high-contrast imaging) [3–4]. Another advantage is that the non-ionizing nature of terahertz radiation presents no major health risks for humans [2–4].

A potential application of terahertz imaging could be in screening passengers and their personal belongings in order to detect various high-risk materials, such as explosives or knives. Although this technology is full of potential, the scientific community has to overcome many obstacles including obtaining high power THz sources and sensitive detectors that operate at room temperature. Currently, real-time imaging at

THz frequencies is primarily carried out using infrared-optimized microbolometer cameras with cryogenically cooled quantum cascade lasers (QCLs) as illuminators, since the thermal background does not have appreciable energy at THz frequencies [2–4].

The challenge in this thesis research is to further demonstrate the potential for high quality imaging in the THz domain and to test operationally an IR camera that has been modified accordingly in producing THz images. The modification of the IR camera involves the replacement of the camera's original Ge lens with a Tsurupica-based lens known from previous research to focus THz radiation efficiently on the focal plane array (FPA). The research concept developed in this thesis supports the establishment of an imaging mechanism consisting of a modified IR camera capable of imaging in the THz domain, a THz-source quantum cascade laser (QCL) operating as an illuminator, and an optics arrangement capable of optimizing the propagation of the laser beam.

## A. RESEARCH OBJECTIVES

The research presented in this thesis aimed to address the following objectives. First, to present the relevant theory in THz imaging via the usage of a modified infrared camera that utilizes microbolometer-based FPA when objects are illuminated by a QCL. Further, characterize the QCL beam characteristics as a function of bias current and analyze the mode hopping phenomenon. Mode hopping causes a change in the output wavelength and establishes electric tunability of QCLs. The final and most important objective was to present real-time imaging capability of the FLIR A20 IR camera in the THz spectral band.

# II. MICROBOLOMETER CAMERA (THERMOVISION FLIR A20M)

## A. OPERATION OF MICROBOLOMETER FPA PIXELS

In the following paragraphs, a brief description of the operational principle behind microbolometer pixels is presented. An analytical description of microbolometer theory is presented in details in [2], [4], [5], and [6]. Uncooled microbolometer FPAs for infrared imaging applications have been investigated since the early 1980s [2, 4, 5]. Although their primary use was in IR radiation, the bolometric effect was applicable to the entire electromagnetic spectrum, and thus microbolometer FPAs can be utilized for the detection of THz radiation [5].

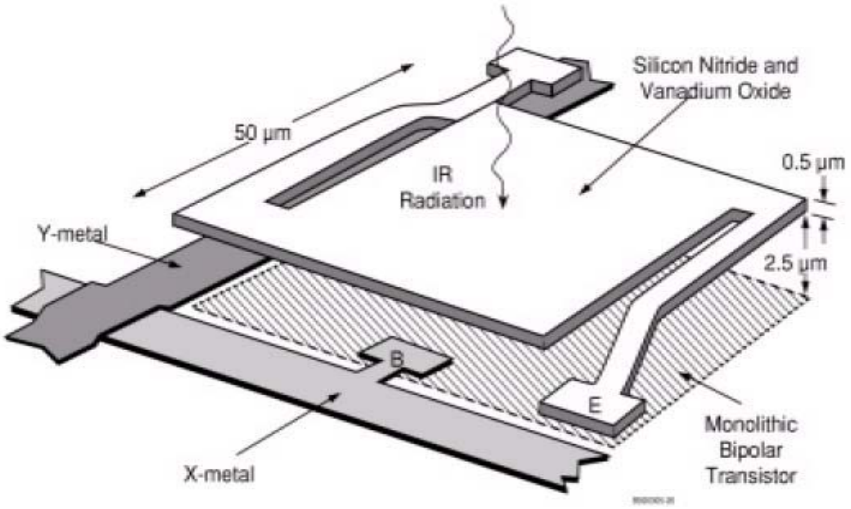


Figure 2. A Schematic Diagram of a Typical MEMS Microbolometer Pixel (From [5]).

A microbolometer pixel, as illustrated in Figure 2, has the ability to detect minor temperature variations that are proportional to the absorbed radiant power (P) by the pixel membrane (silicon nitride). The change in the temperature $\Delta T$ causes an analogous change in the resistance $\Delta R$ of a resistive element (vanadium oxide thin film) that is integrated to the MEMS pixel, which can be expressed by the following linear equation [5]:

$$\Delta R = \alpha R \Delta T , \quad (1)$$

where $\alpha$ is the temperature coefficient of the resistance (TCR) of the resistive film [5]. In order to enhance the sensitivity, microbolometer pixels are manufactured in a fashion that establishes high thermal isolation by reducing the thermal contact to the substrate and preventing convection losses by keeping it in a vacuum. If the heat capacity of each sensing element is C (J/K), for a temperature difference $\Delta T$ between the substrate and the pixel, the absorbed heat Q by each individual sensing element can be expressed as follows [5]:

$$Q = C\Delta T \quad . \tag{2}$$

However, the increase of the temperature in each sensing element-pixel of the substrate causes heat flow to occur. The heat balance equation including the incoming power (P) and considering the system being thermodynamically balanced can be written as [5]:

$$P = G\Delta T + C\frac{d}{dt}\Delta T, \tag{3}$$

where the thermal loss develops with a rate of $G\Delta T$ and where G (W/K) is the thermal conductance. If the incident power is time-dependent $P\sin(\omega t)$ , the steady state response of the microbolometer, after a long time, is given by the formula [5, 7, 8].

$$\Delta T = \frac{\eta P}{G\sqrt{1^2 + (\omega\tau)^2}}\sin(\omega t - \theta), \tag{4}$$

where $\tau=(\frac{C}{G})$ is the thermal time constant, $\eta$ is the absorption efficiency of the sensing area and $\theta = \tan^{-1}(\omega\tau)$ is the phase difference between the incident power and temperature change. The $\eta$ depends on the material used as the membrane in the pixel. From the above equation, one can have an estimate of how a pixel operates when it detects pulse-modulated THz radiation [5]. Microbolometers are configured into an FPA in the camera and different amounts of heating of the pixels can be used to reconstruct the thermal image of a target, as illustrated in Figure 3 [9].

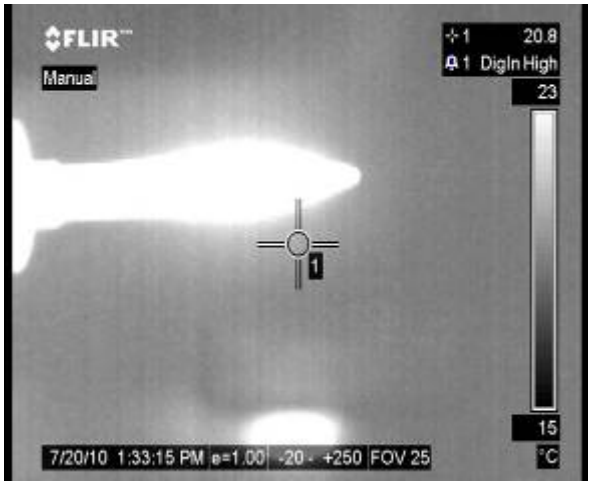


Figure 3. Infrared Image of a Soldering Iron Captured Using the FLIR A20m Camera.

## B. CAMERA OPERATION

The Thermovision FLIR A20m camera is a fundamental part of the THz imaging system. All objects in nature emit thermal radiation if their temperature is above absolute zero. This thermal radiation is usually detected by IR cameras that consequently transform incoming thermal radiation into electrical signal, which is then used by the camera to produce a thermal image [9].

The key parts of the FLIR IR camera are the microbolometer FPA, a Ge lens that focuses the incoming IR radiation on the FPA, and various electronic subsystems equipped with the proper software to collect all the thermo graphical data to recreate the thermal image of the object, as shown schematically in Figure 4. The next step is to display all the collected data (thermal image) of the target on a display device such as a LCD screen [9].

The main differences between standard digital cameras used in photography and IR cameras are the optics and type of FPAs to match the required wavelength bands. The camera used in this thesis work, for which the FPA is composed of microbolometer pixels, is manufactured by various materials that are sensitive to IR radiation. Each pixel produces an analog signal depending on the absorbed radiation power, which is then digitized using an A/D converter with resolution up to fourteen bits [9].

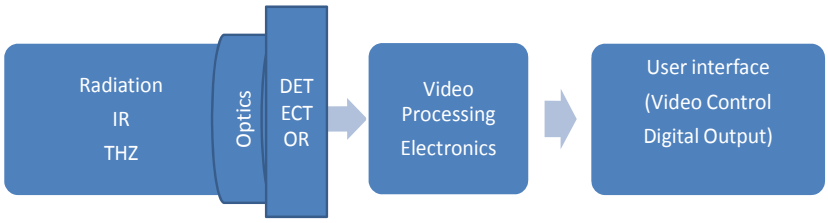


Figure 4. Simplified Block Diagram of a Typical IR/THz Camera (After [9]).

In this work, THz radiation is focused on the FPA using a Tsurupica lens and the FPAs convert the radiation power to electrical signals, which are processed by the on-board electronics to generate an image.

## C. TECHNICAL SPECIFICATIONS OF FLIR A20M CAMERA

The microbolometer camera used in this work was a FLIR A20M (see Figures 5 and 6) with silicon nitride (SiN)-based pixels. The initial part of this research was to become familiarized with the FLIR A20M camera. In this work, it was necessary to understand the advanced features of the camera for image manipulation.


Figure 5. Photograph of the FLIR Thermovision A20M Infrared Camera.


Figure 6. Photograph of the Back Panel of the FLIR A20M Infrared Camera.

The major technical specifications of the camera are listed in Table 1.

| | |
|---|---|
| **Detector Type** | Focal Plane Array (FPA)<br>Uncooled Microbolometer |
| **Field of View** | 25◦ x 19 ◦ / 0.3 m |
| **Spatial Resolution** | 2.7 milirad |
| **Temperature Range** | Range: -20$^{0}$ C to + 250$^{0}$ C |
| **Thermal Sensitivity** | 0.12$^{0}$ C at 30$^{0}$ C |
| **Measurement Modes** | Area , Spot , Difference |
| **Image Resolution** | 60 x 120 pixels |
| **Spectral range** | 7.5 – 13 μm |
| **Focusing** | Internal built-in motor |
| **Storage Capability** | 50 – 100 images |

Table 1. Main Technical Features of the FLIR A20M Camera (After [9]).

Throughout the experiment, the camera was interfaced to a desktop computer via a firewire cable. The software package that was procured with the camera was installed to the desktop computer for acquiring and displaying the images. Additional software was also obtained from the manufacturer for extracting the stored images. Another issue that limited this work's image processing capabilities was that although the camera had a maximum storage capacity of one hundred pictures, it could only save pictures as JPEG files. It would have been rather useful if the camera offered the users the option of storing images as bitmap files or another suitable file type with higher resolution. The operation of the camera was performed through a display menu on the computer screen. This

approach proved to be quite convenient. Another advantage of the camera was the fact that the firewire connection covered the power supply requirements as well, so no extra connections were necessary.

THIS PAGE INTENTIONALLY LEFT BLANK

# III. QUANTUM CASCADE LASER (QCL)

## A. BACKGROUND

Various approaches have been explored to generate electromagnetic radiation in the 0.1 to 10 THz spectral range, as illustrated in Figure 7. One of the most promising approaches is the quantum cascade laser (QCL), due to its relatively high power and small form factor [2–4]. High power lasers are needed for imaging at relatively long standoff distances. However, one of the main disadvantages is that it requires cryogenic cooling to minimize thermal excitation of electrons between narrow energy levels (~ 10 meV) required for generating THz photons.

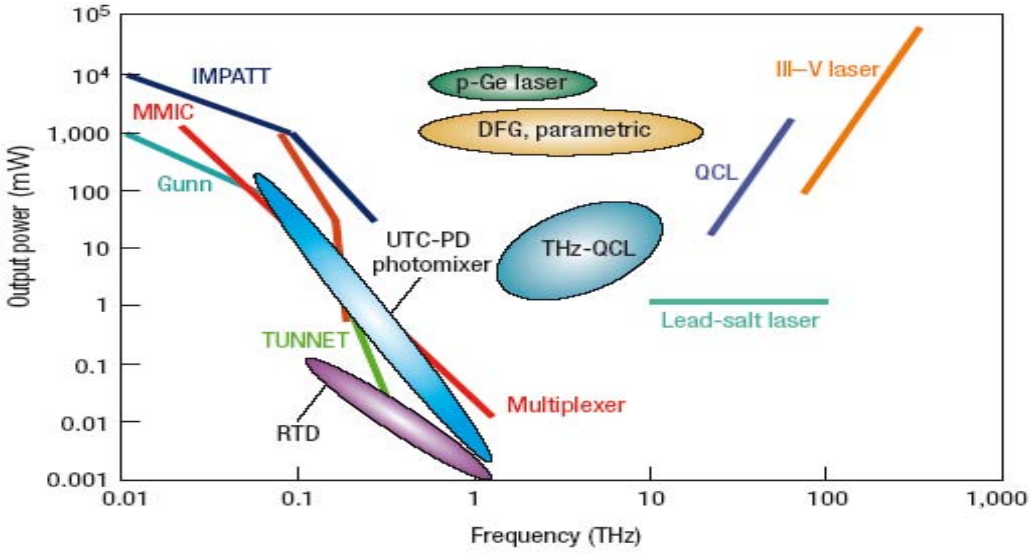


Figure 7. Methods of Producing THz Radiation. "DFG" Refers to Difference-frequency Generation (From [2–10]).

The operational concept of this kind of laser was originally introduced by Kazanof and Suris in 1971 [11]. QCLs operation is based on the concept of intraband transitions that have the ability to emit photons [12]. The QCL utilizes the quantum well structure to generate photons when an electron performs intraband transitions inside a multiple quantum well structure, as schematically illustrated in Figure 8 [12].

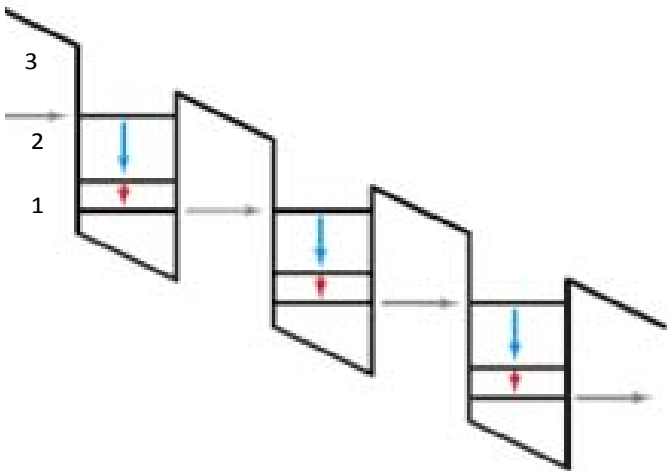


Figure 8. A Simplified Schematic of a QCL (From [13]).

Electrons are first injected into the energy level of the quantum well 3 in Figure 8, which drops to level 2 via photon emission and then relaxes to the ground state (level 1). However, in order to maintain the population inversion between levels 2 and 3, the electrons in level 2 should undergo rapid transition to level 1. In the case of IR QCLs, this is achieved by setting the energy difference between levels 1 and 2 equal to the optical phonon energy of the laser material (~30 meV for GaAs). This process is repeated when the electron enters the next well, enabling each electron to produce as many photons as the number of quantum wells. However, it is difficult to extend this approach to THz QCLs since the THz phonon energies are small compared to typical optical phonon energies. The use of bound-to-continuum transitions was successfully employed for the fabrication of THz QCLs [11–12]. The operation of the QCL used in this work is based on the latter approach.

## B. LASER CHARACTERISTICS

The structure and dimensions of the QCL used in this work is shown in Figure 9 [14]. The length of the laser cavity is about 2.4 mm.

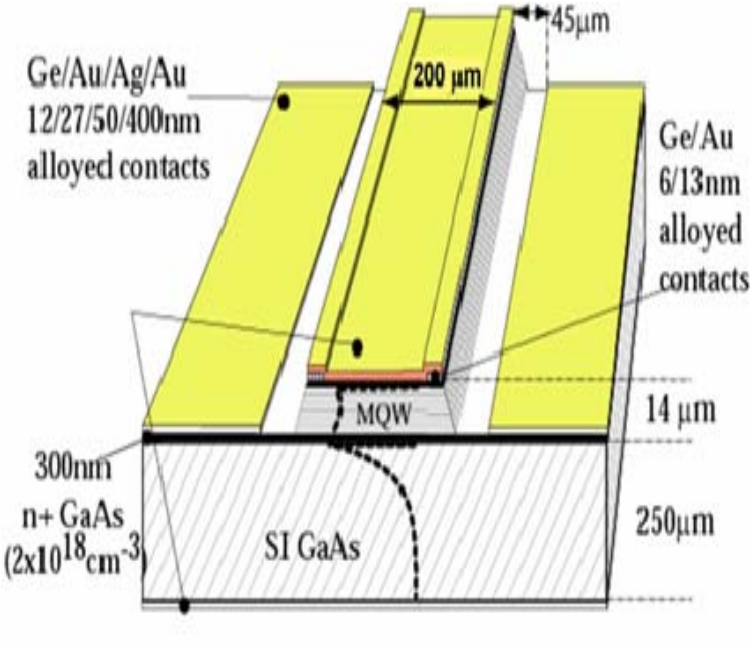


Figure 9. Waveguide of Bound-to-continuum 2.7 THz QCL Used in this Experiment (From [14]).

The characteristics of the QCL under different operating conditions were first probed using a FTIR spectrometer fitted with a THz beam splitter and DTGS detector with a polyethylene window. The main objective in this measurement was to characterize spectral content of the laser beam and determine the laser output power as a function of bias current. The laser was operated in pulse mode at 100 kHz with a 10% duty cycle to limit the excessive heating of the active region due to larger bias voltage and current typically needed for QCL operation. Measurements were performed by sending a collimated laser beam to the external port of the FTIR using a parabolic and a flat mirror as depicted in Figure 10. Furthermore, in order to maintain a steady operating temperature of the laser and avoid excessive Joule heating effects, only one scan per measurement was carried out. It was possible to maintain a good signal-to-noise ratio during the measurement due to relatively high laser power.

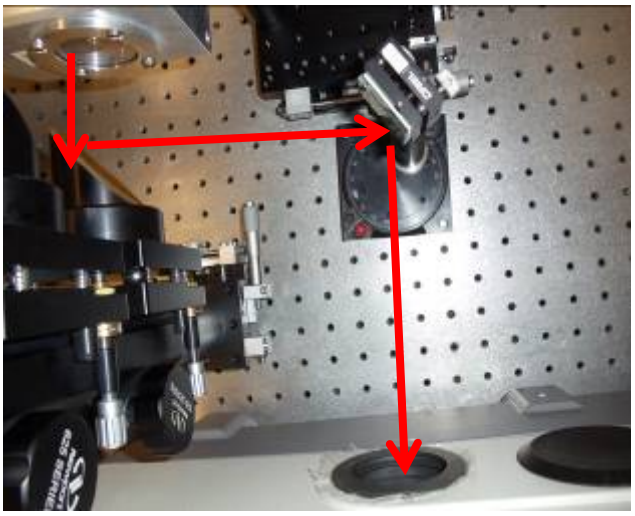

Figure 10. Optics Used in the FTIR Measurement; Red Arrow Indicates the Path of the Laser Beam.

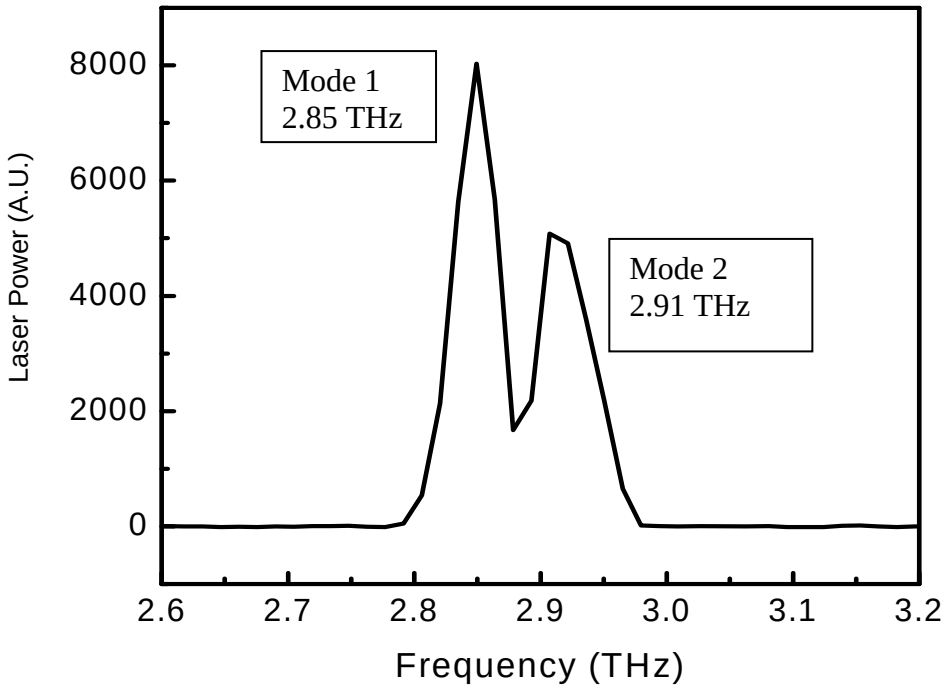


Figure 11. Measured Laser Output Signal vs. Frequency.

Figure 11 shows the measured intensity of the laser beam as a function of THz frequency at 1.4A bias current. The highest resolution of the FTIR in this spectral band is 1 $cm^{-1}$ (or 0.3 GHz) and used in these measurements. It can be clearly seen that the output of the laser contained two lasing modes at 2.85 and 2.91 THz with nearly equal intensity. It is possible to calculate the frequency difference between the modes in a semiconductor laser using the length of the cavity (L) and refractive index ($n_r$) of the material using the formula

$$2Ln_r = m\lambda \tag{6}$$

This equation can be rewritten in terms of frequency, f, (more appropriate in the THz band) of the laser light as

$$2Ln_r f = mc \tag{7}$$

where c is the speed of light. This implies that the frequency separation ($\Delta f$) between the successive modes is given by

$$2Ln_r \Delta f = c \tag{8}$$

Since the length (L) of the laser was unknown originally, it was measured using a calibrated optical microscope. Figure 12 shows the optical micrograph of the top view of the laser with the measured length of 2.4 mm.

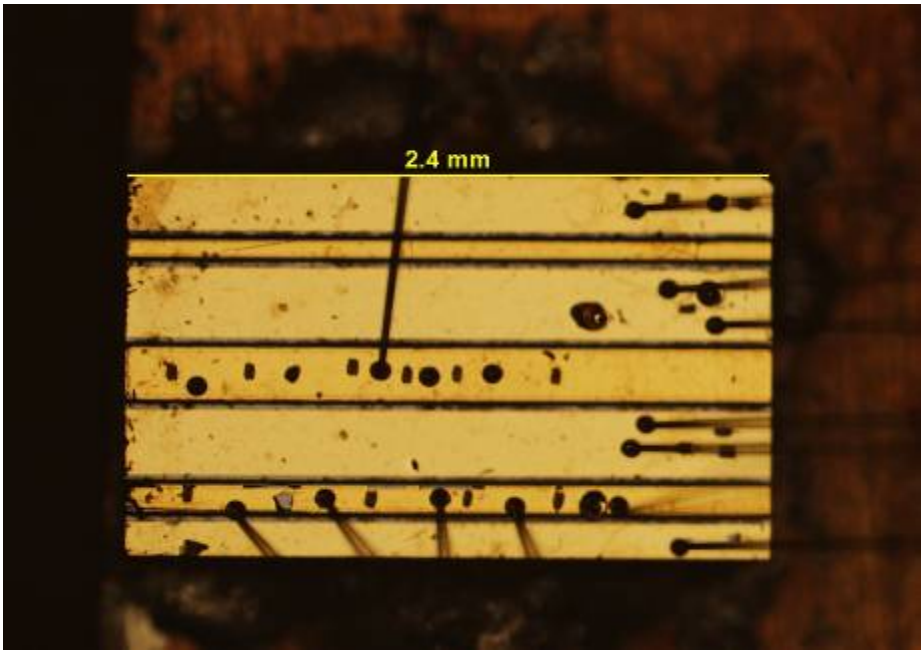


Figure 12. Optical micrograph of the QCL Used in this Thesis.

Taking the index of refraction of GaAs to be 3.4, the frequency difference between the two modes was calculated using Equation 8 and equaled 0.18 GHz. However, the measured value for the two peaks observed in the measurement was found to be about 0.68 GHz. Previous observations of the mode structure of THz-QCLs with similar cavity lengths showed the measured mode separation to be about 0.19 GHz [15] (which is comparable with the calculated value of 0.18 GHz). One reason for the discrepancy is that the low resolution of the spectrometer, 1 $cm^{-1}$ or 0.3 GHz, does not resolve the successive modes of the laser. In addition, gain curve of the laser can affect the strength of the modes. Further investigation is needed to confirm this observation by increasing the resolution of the FTIR spectrometer beyond the current maximum, which is beyond the scope of this thesis.

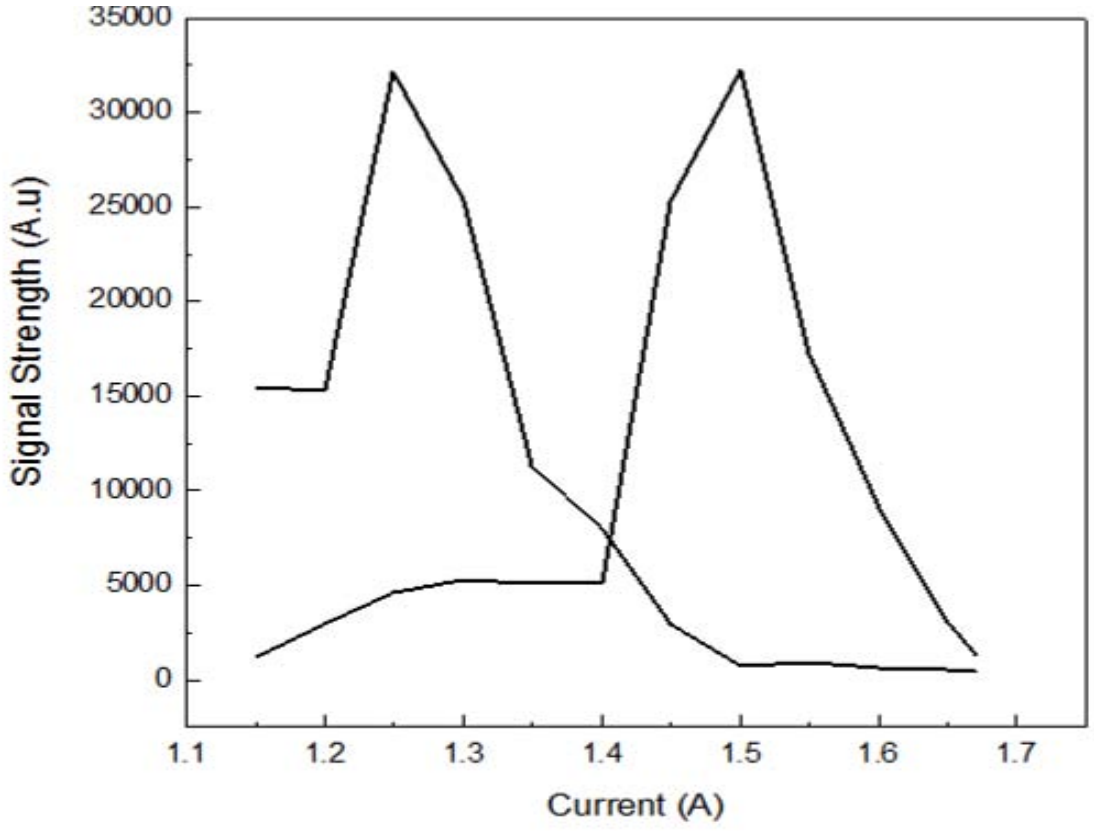


Figure 13. Measured Signal vs. Bias Current for the Two Modes at 2.85 and 2.91 THz.

In Figure 13, the measured signal as a function of frequency is clearly depicted, and in particular, one can observe the appearance of two modes for two specific frequency lasing values of 2.85 and 2.91 THz.

THIS PAGE INTENTIONALLY LEFT BLANK

# IV. TERAHERTZ IMAGING

## A. QCL OPERATION

A crucial component of THz imaging for this work involved the use of a cryogenically cooled (~10 K) 2.7 THz QCL using a closed-cycle refrigeration system (CCR). In addition, the QCL was mounted on a copper black heat sink that was attached to the cooling system's cold finger. During the operation of the cryostat, the chamber that contained the QCL was kept under vacuum using a Varian Turbo V301-AG pump. The temperature of the closed finger was monitored using a temperature controller.

During the measurements, the QCL was operated in pulsed mode using an Agilent 8114 pulse generator with maximum current of 2 A. However, due to previous extensive research work on QCL biasing, the majority of settings were preselected; this work's focus and interest are only on adjusting the bias current, and there were a limited number of settings such as duty cycle of the injected current pulses [2–4]. The duty cycle values during the experiment varied from 10% to 22 %, and after a series of measurements and trials, the optimal duty cycle value was found to be 22%. The optimal current value for the imaging experiment was found to be about 1.25 A to minimize the excessive heating of the laser while obtaining high enough power. A detailed description of the QCL operation can be found in [2], [3], and [4].

## B. OPTIMIZATION OF OPTICS

In this thesis, the main scope was to demonstrate feasibility of the use of a FLIR A20M camera for THz imaging. In order to achieve this, the optical arrangement developed by the Sensor Research Laboratory (SRL) research group with some fine tuning was utilized [2–4].

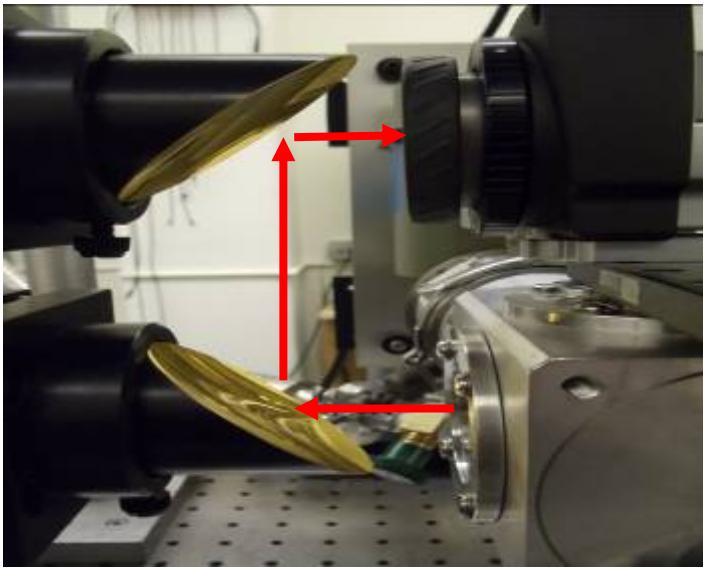

Figure 14. Experimental setup where two parabolic reflectors are used to collect, focus and steer the laser beam to the camera Lens. The optical path of the THz beam is depicted in the above photograph.

The aim was to expand the laser beam to cover the extent of the object to be illuminated. This was achieved by placing the laser on the opposite side of the focal point of an off-axis parabolic mirror, as illustrated in Figure 14. The parabolic mirror used for expanding the QCL beam has a focal length of 50.8 mm with gold coating for high reflectivity in the THz spectral range. Then, the object was placed above the parabolic mirror (see Figure 15) and the THz passing through the object was collected using a second off-axis parabolic mirror with a focal length of 101.6 mm. The object was placed on the same side of the focal point of the second parabolic mirror to collect the diverging THz beam from the first mirror.

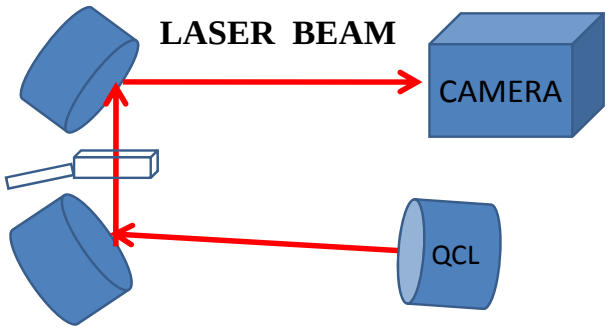


Figure 15. Schematic of the Imaging Setup. The Two Parabolic Gold-plated Mirrors are mounted on the Same Post for Convenience in Alignment.

A 1-inch diameter bi-convex Tsurupica lens with focal length 20 mm was utilized to focus the image on the FPA by replacing the original Ge lens of the camera. Measured transmission characteristics of Tsurupica shows that it has good transmission in THz range of interests, as well as in visible ranges, as illustrated in Figures 16 and 17, respectively [16].

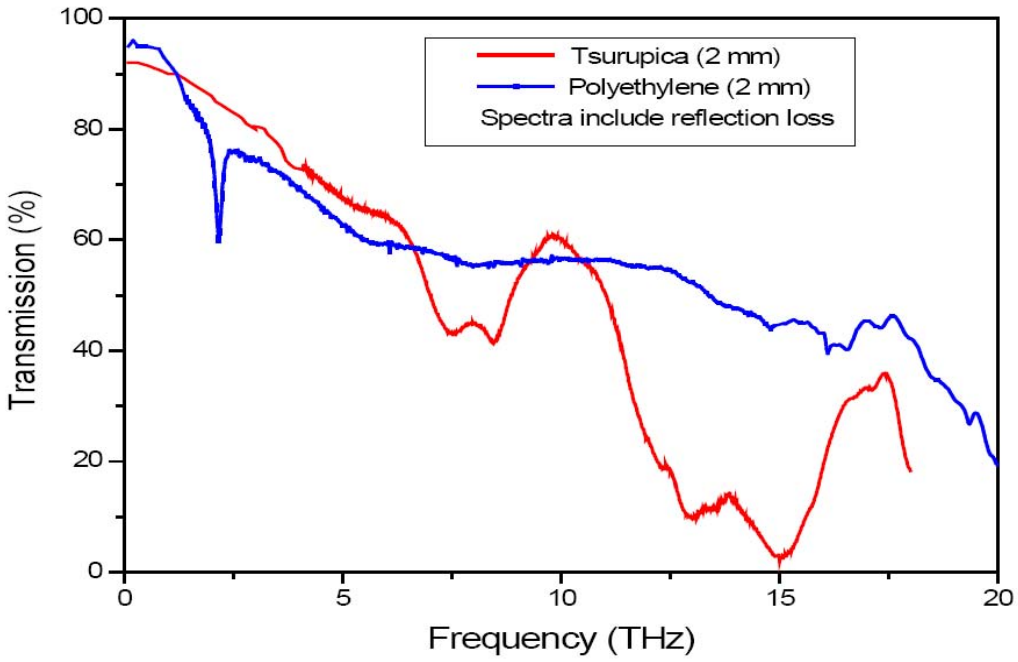


Figure 16. Transmission of Tsurupica and Polyethylene in THz Spectral Range (From [16]).

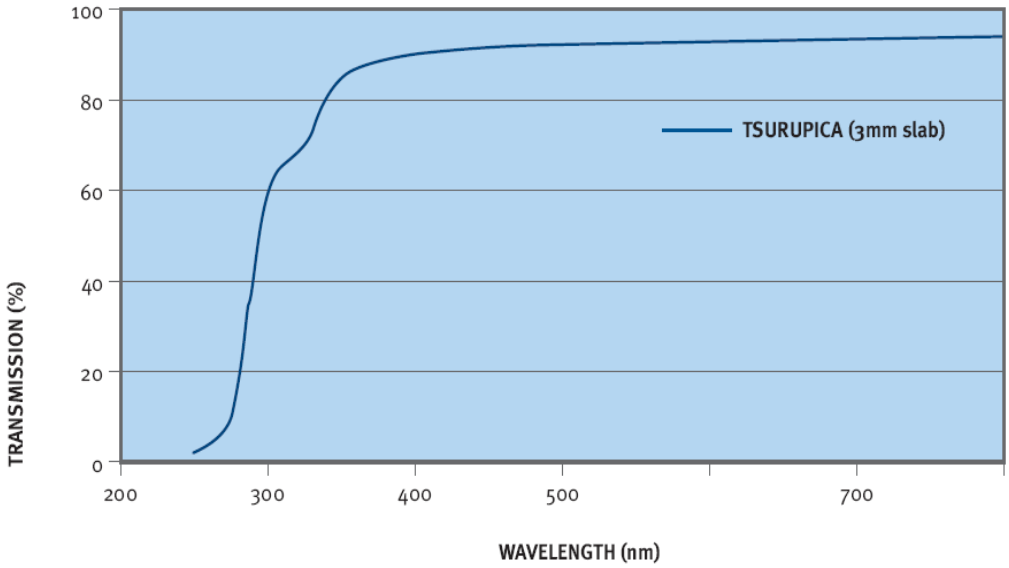


Figure 17. Transmission of Tsurupica in Visible Spectral Range (From [16]).

Since the focal length of the Tsurupica lens that was available to this work was different from that of the Ge lens that came with the camera, a number of adjustments to the placement of the lens in the original lens holder were required to achieve proper focusing of the object on the FPA.

The metallic blade covered with white plastic was placed on the average midway between the two reflectors as in earlier imaging experiments using the IR 160 microbolometer camera [2]. The exact distances used during the imaging are listed below.

- Cryostat window to lower edge of parabolic mirror: 20 mm
- Lower parabolic mirror to upper parabolic mirror (upper to lower edges): 30 mm
- Edge of upper parabolic mirror to camera: 5 mm

## C. THERMOVISION FLIR A20 CAMERA PERFORMANCE AND RESULTS

Initial imaging experiments were carried out to detect the laser beam from the THz QCL with placing the Tsurupica lens at the bottom of the original lens holder that came with the camera. The THz radiation from the laser is highly divergent due to its small aperture (10 μm) compared to the wavelength of the laser of about 106 μm. Thus, the THz beam was first collimated using the first parabolic mirror. This was achieved by sending the reflected THz beam from the first mirror to the FTIR with the help of a flat mirror. This provided a convenient way of adjusting the position of the mirror to keep the laser at the focal point since the FTIR signal was at its maximum when the beam was collimated. Figure 18 shows an image of the laser beam captured using the camera. It can be clearly seen from the image in Figure 19 that there are a number of circular rings around the central spot, primarily due to diffraction of the long wavelength, $\lambda$ = 106 μm of THz radiation from the 0.375 " diameter (D) slit in the camera.


Figure 18. An Image of the Collimated THz Beam Focused Using the Tsurupica Lens.

The calculated diameter of the central spot ($2.44\lambda f/D$) is about 270 μm (see Figure. 19), which is close to the measured value of 300 μm using the dimensions of the pixels in the array. The focal length, f, of the lens is 20 mm.

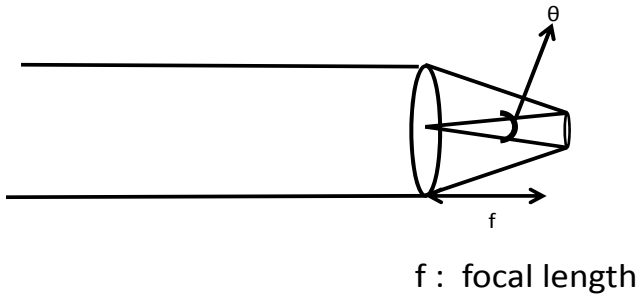


Figure 19. A Schematic of the Diffracted Laser Beam from the Camera Lens Showing the Airy Disc.

The detection of the laser beam using the camera is the first step needed before beginning the imaging of objects. Relatively high signal strength of the image of the laser beam indicates that the pixels in the camera efficiently absorb THz radiation. The next step was to arrange the two parabolic reflectors as schematically shown in Figure 13, with the object located in between the mirrors. For the subsequent measurements, the operating conditions of the THz QCL were modulation frequency of 100 kHz with 22 % duty cycle and pulse generator output impedance of 10Ω. The amplitude of the bias current value was kept at 1.25 A to achieve the highest possible power, while keeping the heating effects at a minimum. A metallic utility knife blade covered with plastic opaque tape on both sides was used as the object to be imaged (See Figures 20, 21).

Figure 20. Photograph of the Metallic Blade.

One of the reasons why the metallic blade was used for these measurements is that the sharpness of the blade would provide a good starting basis to evaluate the performance of the camera. In addition, the fact that the metallic blade cannot be penetrated by the THz radiation in conjunction with the gap in the central part of the blade is useful in evaluating the performance of the camera in THz imaging.

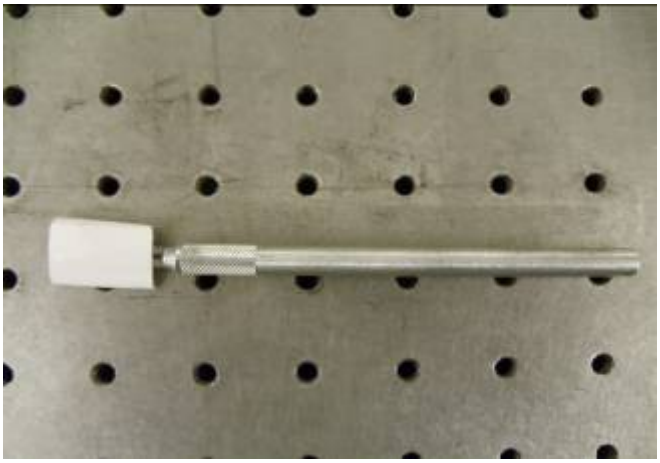

Figure 21. Photograph of the Metallic Knife Blade Wrapped in White Plastic Tape.

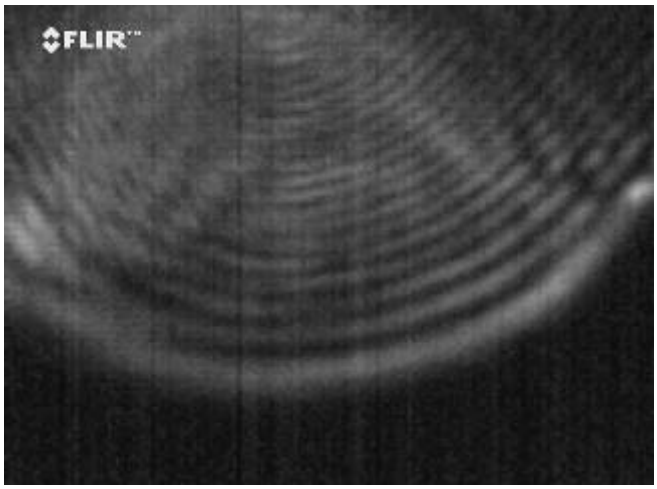


Figure 22. Image of the expanded laser beam covering nearly all of the FPA using the two parabolic reflectors.

Figure 22 shows the image of the laser beam after reflecting from the two mirrors. An interesting feature of Figure 22 is the appearance of a large number of diffraction fringes that are spread out across the FPA. This implies that a diverging THz beam is arriving at the camera and the circular nature of the fringes indicates again that the lens is responsible for the diffraction fringes. Figures 23, 24, and 25 demonstrate images of the metallic blade captured under different camera settings, namely the camera settings that were adjusted to improve the quality of images. The parameters include emissivity

background intensity and temperature resolution. For all the images in this thesis, the palette used was the gray hot palette and the emissivity value was set to be one.

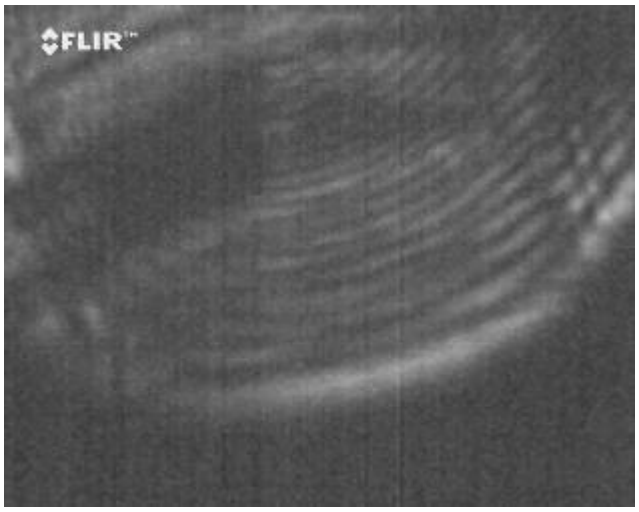


Figure 23. THz Image Obtained After Inserting the Utility Knife Wrapped in White Plastic Tape Between the Two Mirrors.

One of the advantages of THz radiation is the high degree of reflection/absorption from metallic objects and penetration through nonmetallic materials (i.e., opaque plastic tape, with low attenuation). In Figure 23, the contrast between the opaque plastic tape and the metallic blade is quite clear, constituting the metallic blade to be detectable; however, the low output power of the QCL limits the signal-to-noise ratio.

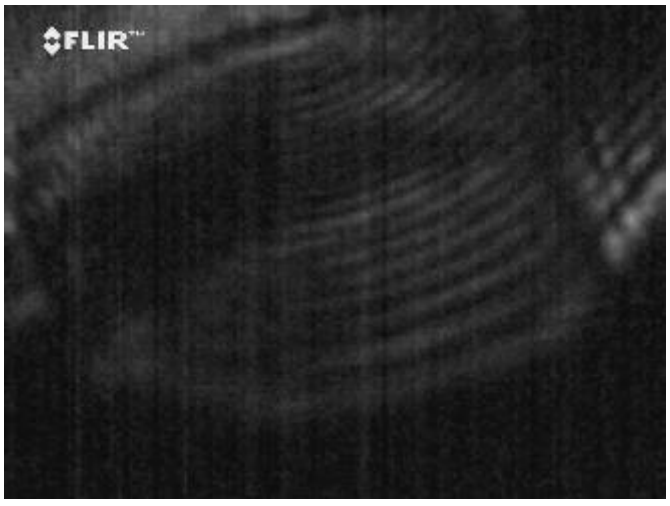


Figure 24. THz Image of the Utility Knife with Contrast Adjusted.

In Figure 24, a black and white contrast of high intensity was chosen to offer a more accurate perception of the metallic blade shape and a better sense of the relative position of the metallic blade internally in the plastic tape.

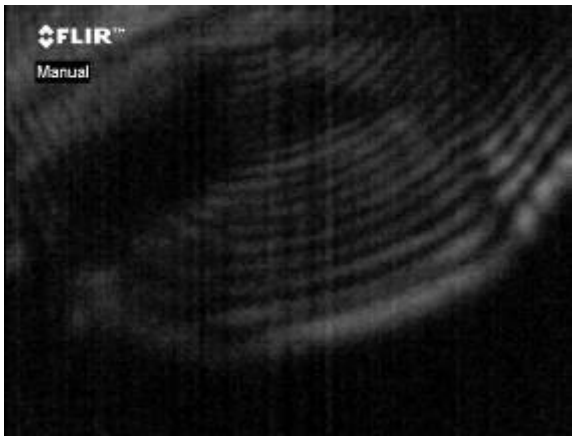


Figure 25. One frame of real time video taken by the camera.

Figure 25 was exported from one of the videos captured during this research to evaluate experimentally the FLIR A20M camera, which clearly demonstrates the high quality real-time THz imaging that can be accomplished using the camera.

An important factor that enhanced the quality of the images was the timing when they were captured relative to the switching of the QCL. The QCL provides the highest power during the first few seconds of operation and then starts to degrade due to Joule heating. Note that the typical average power input to the laser is about 4 Watts and most of it dissipates as heat. Continued operation of the laser increases the temperature of the cryostat by about 10 K, which reduces the output power.

The captured images in Figures 23, 24, and 25 clearly underline the high potential of THz imaging using a FLIR A20M microbolometer camera. The successful results from the testing of the plastic opaque tape as covering material, despite the low laser output power, signals the need for further research on different concealing materials such as fabric and different types of plastic.

# V. CONCLUSIONS AND RECOMMENDATIONS

In this thesis, real-time THz imaging was accomplished using a FLIR A20M microbolometer camera along with a THz QCL as an illuminator. Initially, the spectral and electrical characterizations of the QCL were performed. It was found that QCL had two distinct modes depending on the bias current. Both modes were found to have nearly equal output power and the mode at low current was used for imaging to minimize the heating effects that affected the laser output. The FLIR A20M camera was used to image the collimated laser beam using a parabolic mirror. Images of the laser beam showed diffraction fringes, and their origin was found to be associated with the circular lens used for focusing the THz beam on the FPA.

With the successful imaging of the THz laser beam, the camera was used for imaging concealed objects. This required the use of an additional parabolic mirror to expand the laser beam to illuminate the object to be imaged. The most challenging part during this task was to identify the optimal optics arrangement, considering the output power of the laser is only 1 mW, a parameter that practically sets constraints on the quality of imaging. However, real-time images of concealed objects were successfully obtained by optimizing the optics as well as the laser power.

Further improvement of the image quality, require lasers with high output power. This will not only enhance the signal-to-noise ratio but also the standoff distance. In addition, reflection mode imaging can be performed, which will result in a more compact system than the transmission mode. An additional enhancement can be made by designing FPAs that are optimized for THz detection by increasing the pixel size from the current 50 $\mu m^2$ to larger than the THz wavelengths of interest. These activities are currently in progress at SRL and will undoubtedly enhance the quality of images.

THIS PAGE INTENTIONALLY LEFT BLANK

# LIST OF REFERENCES


[1] Advanced Photonix, Inc. The Electromagnetic Spectrum. 15 December 2007 http://www.advancedphotonix.com/ap._products/terahertz_whatis.asp.

[2] B.N. Behnken, Real-Time Terahertz Imaging using a Quantum Cascade Laser and Uncooled Microbolometer Focal Plane Array, Ph. D. Dissertation, Naval Postgraduate School, Mar. 2008.

[3] Hi Quing, H. Callebaut, E. Duerr, K. Konistis, S. Kumar, J. Montoya, et al. Terahertz Quantum Cascade Lasers and Electronics. 2003 Materials Research at MIT (2003).

[4] K. W. Buchanan, Real Time Imaging Analysis Using A Terahertz Quantum Cascade Laser and a Microbolometer Focal Plane Array, M.S. Thesis, Naval Postgraduate School, December 2008.

[5] P. W. Kurse, “Principals of uncooled infrared focal plane arrays,” in Semiconductors and Semimetals 47: Uncooled Infrared Imaging Arrays and Systems, P.W Kurse and D.D Skatrud, ed. (Academic Press, San Diego, 1997).

[6] M. Rochat, L. Ajili, H. Willenberg, J. Faist, H. Beere, G. Davies, E. Linfield and D. Ritchie, "Low-threshold terahertz quantum-cascade lasers," Appl. Phys. Lett. 81, 1381–1383 (2002).

[7] G. Scalari, L. Ajili, J. Faist, H. Beere, D. Ritchie, E. Linfield, G. Davies, "Far-infrared ($\lambda$=87$\mu$m) bound-to-continuum quantum cascade lasers operating up to 90K," Appl. Phys. Lett. 82, 3165–3167 (2003).

[8] E.L. Dereniak and G.D. Boreman, Infrared Detectors and Systems, John Wiley and Sons, New York, NY, 1996.

[9] FLIR Company, 2010, FLIR Automation Guidebook, 10–15.

[10] M. Tonouchi, “Cutting edge terahertz technology,” Nature Photonics I, 97–105 (2007).

[11] R. S. Quimby, “Photonics and Lasers. An Introduction,” Wiley-Interscience, 2006.

[12] W. T. Silvfast, Laser Fundamentals Second Edition, Cambridge University Press, 2004.

[13] Encyclopedia for Lasers and Technology, http://www.rp-photonics.com/quantum_cascade_lasers.html , accessed on August 2, 2010.

[14] Agilent Laboratories Imaging at 3.4 THz with a Quantum Cascade Laser from Power Point presentation, (January 2004).

[15] J. Faist, L. Ajili, G. Scalari, M. Giovannini, , M. Becki, , M. Rochati, , Harvey Beere , A. Giles, E. Davies . H. Linfield and D. Ritchie, Terahertz Quantum Cascade Lasers, The Royal Society, No. 1815, The Terahertz Gap: The Generation of Far-Infrared Radiation and its Applications pp. 215-231, (February 15, 2004).

[16] Microtech Instruments, http://www.mtinstruments.com/thzlenses/index.htm accessed on September 2010.

# INITIAL DISTRIBUTION LIST

1. Defense Technical Information Center
   Ft. Belvoir, Virginia

2. Dudley Knox Library
   Naval Postgraduate School
   Monterey, California

3. Graduate School of Engineering and Applied Sciences
   Naval Postgraduate School
   Monterey, California

4. Professor Gamani Karunasiri
   Department of Physics
   Naval Postgraduate School
   Monterey, California

5. Assistant Professor Dragoslav Grbovic
   Department of Physics
   Naval Postgraduate School
   Monterey, California

6. Professor and Chairman Andres Larraza
   Department of Physics
   Naval Postgraduate School
   Monterey, California

7. Ioannis Nellas
   Naval Postgraduate School
   Monterey, California